

Kondo effect and channel mixing in oscillating molecules

J. Mravlje¹ and A. Ramšak^{2,1}

¹*Jožef Stefan Institute, Ljubljana, Slovenia and*

²*Faculty of Mathematics and Physics, University of Ljubljana, Slovenia*

We investigate linear transport through a molecule in the Kondo regime and with the tunneling to the electrodes which is asymmetrically modulated by the position of the molecule. We model this system by the two-channel Anderson model with phonon-assisted hybridization. We present the results of two functional forms of modulation: the spin at the molecular orbital is always screened by the even conduction channel in the case of exponential modulation, while it is screened by the even or odd channel (depending on the coupling constant) in the case of linear modulation. The softening of the phonon mode occurs due to the gain in kinetic energy by the dynamical breaking of the inversion symmetry and is not directly related to the Kondo correlations, *i.e.*, it occurs also for vanishing repulsion, $U \rightarrow 0$. We discuss also the influence of perturbations which explicitly break the inversion symmetry. At regimes where the frequency of the soft mode decreases below the magnitude of such perturbation, the molecule is abruptly attracted to one of the electrodes; this is an example of increased generalized susceptibility as a consequence of the coupling to a phonon mode. In this regime the Kondo temperature is drastically enhanced simultaneously with suppressed conductance through the molecule.

PACS numbers: 72.15.Qm, 73.23.-b, 73.22.-f

I. INTRODUCTION

The Kondo effect, the hypernym for processes related to the increased scattering rate off impurities with internal degrees of freedom, is manifested in mesoscopic systems as increased conductance at bias and temperatures low compared to the Kondo temperature. Experimentally, the Kondo effect has been discerned in transport through quantum dots¹, atoms, and molecules^{2,3,4,5,6,7,8}. Specific to experiments with molecules is the influence of the electron-phonon coupling; in measurements both breathing-like oscillations and vibrational modes where the molecule oscillates with respect to the leads have been identified as side-peaks in the non-linear conductance^{4,5,6}. Besides explaining the features revealed in the non-linear transport measurements, the electron-phonon coupling can also account for the anomalous dependence of the Kondo temperature on changing the gate voltage at zero bias^{8,9,10,11}. Since the electrode-molecule junctions are candidates for devices such as molecular diodes, switches, and rectifiers the research in this field is increasing despite its complexity and difficult experimental characterization^{12,13,14}. Recently, also a quantum phase transition was observed in such system¹⁵. Understanding the behavior of the simplified theoretical models is essential to enable the interpretation of the experimental results.

Here we are interested in the influence of the electron-phonon coupling in the Kondo regime where there is predominantly a single electron occupying the molecular orbital. We concentrate on the case where the tunneling barriers from the molecular orbital to the leads are affected by the displacement x of the molecule from the halfway between the leads, as depicted schematically in Fig. 1. The tunneling towards the left and right leads is determined by overlap integrals $V_{L,R}(x)$ which ex-

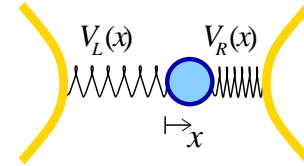


Figure 1: (Color online) Schematic plot of the model device.

panded to lowest order in x read $V_{L,R}(x) = V(1 \mp gx)$, where V sets the scale of the tunneling and the electron-phonon coupling constant g its alteration due to the displacement¹⁶.

Assuming the leads are identical, the system is symmetric with respect to inversion. On that account it is convenient to introduce symmetric and antisymmetric combinations of states in the leads forming with respect to inversion the even and odd conduction channels, respectively. In the linear approximation introduced above, the even channel is coupled to the molecule directly and the odd channel is coupled to the molecule via a term proportional to gx . The asymmetric modulation of tunneling by displacement hence couples the molecular orbital to additional conduction channel.

The consequence of the coupling to two channels is that the low energy behavior is characterized by the two-channel Kondo model^{9,17} (2CK) in which the screening of the spin occurs in the channel with the larger coupling constant. If the couplings match, the non-Fermi liquid 2CK fixed point occurs as a consequence of the overscreening. In simulations based on the numerical renormalization group such a fixed point has been found¹⁸ for the linearized model discussed here.

The renormalization of phonons is also interesting: quite generally, the characteristic frequency of the os-

cillations decreases with increasing electron-phonon coupling. For instance, in the case of the standard Anderson-Holstein model the softening of the phonon mode is related to the increased charge susceptibility^{19,20}, which occurs due to the dynamical breaking of the particle-hole symmetry in the regime of negative effective repulsion. In the present case the softening occurs likewise, however it is related to the dynamical breaking of inversion symmetry⁹. In analogy to the results for the Anderson-Holstein model the increased susceptibility towards the breaking of the inversion symmetry is expected. In the variational approach (the model II of Ref. 21) the instability towards such a breaking has been found indeed. It has been asserted there also that the asymmetric ground state with large average displacement from the halfway between the leads would result in the suppression of conductance.

In this work we extend the existing analysis in two ways: (i) motivated by the lack of the inversion symmetry of typical experimental devices we include the explicit inversion symmetry breaking term – we set the strength of the breaking proportional to the dimensionless ζ ; (ii) we check which features of the linearized model (for brevity, LM) persist in arguably more realistic ‘exponential’ model (EM), in which the tunneling barriers towards left and right leads, $V_{L,R}(x) = V \exp(\mp gx)$, are exponentially dependent on the relative displacement from halfway between the leads. In particular, we point out that in EM the coupling to the even channel is invariably stronger than the coupling to the odd channel. The 2CK fixed point is thus inaccessible in EM and occurs in LM only as an artifact of the linearization.

Both directions of research have been pursued in the context of nanoelectromechanical systems^{22,23,24} and including only lowest orders in tunneling thereby ignoring the Kondo correlations. Similar approach has been taken in the analysis of the influence of pair tunneling in the negative effective repulsion regime of the Anderson-Holstein model^{25,26}. On the other hand, the influence of the exponential alteration of tunneling in the Kondo regime, but taking the displacement $x(t)$ not as a dynamical variable but as an externally controlled parameter, has been analyzed in Ref. 27.

The paper is organized as follows. In the next section we describe the models under consideration in more detail. We have performed the numerical calculations using Wilson’s numerical renormalization group (NRG) and projection operator method of Schönhammer and Gunnarsson’s (SG) which we briefly describe in Section III. In Section IV we give the analytical and in Section V the numerical results. We conclude by critically commenting the obtained results and their applicability. The comparison between the NRG and SG results is given in Appendix A followed by Appendices B and C containing the derivations regarding the Schrieffer-Wolff transformation and the conductance formulas.

II. MODELS

To model the system we use the extension of the Anderson Hamiltonian

$$H = H_{\text{mol}} + H_L + H_R + H_{\text{vib}} + H', \quad (1)$$

where H_{mol} describes the isolated molecule, H_L and H_R the left and right leads, respectively, H_{vib} the vibrational mode and H' the displacement-modulated coupling of the molecular orbital to the leads. The molecule consists of a single orbital with energy ϵ , which is in experiment modulated by the gate voltage. The repulsion between the two electrons simultaneously occupying the orbital is U ,

$$H_{\text{mol}} = \epsilon(n_{\uparrow} + n_{\downarrow}) + Un_{\uparrow}n_{\downarrow}, \quad (2)$$

where the number operators $n_{\sigma} = d_{\sigma}^{\dagger}d_{\sigma}$ count the number of electrons in the orbital with spin $\sigma = \uparrow, \downarrow$. The symbols $c^{(\dagger)}$, $d^{(\dagger)}$ denote electron annihilation (creation) operators in the leads and molecular orbital, respectively. The oscillator part is

$$H_{\text{vib}} = \Omega a^{\dagger}a, \quad (3)$$

describing the oscillations with frequency Ω and a^{\dagger} is the boson creation operator. The left and right leads are described by bands of noninteracting electrons $H_{\alpha} = \sum_{k\sigma} \epsilon_k n_{k\alpha\sigma}$ for $\alpha = L, R$, respectively, where $n_{k\alpha\sigma} = c_{k\alpha\sigma}^{\dagger}c_{k\alpha\sigma}$ is the number operator for electrons with spin σ and wave-vector k ; ϵ_k is the dispersion of the band in the lead α . The chemical potential is set to the middle of the band ($\mu = 0$) corresponding to half-filling regime where the molecule is on average singly occupied. In NRG calculations a flat band with constant density of states $\rho = 1/(2D)$ and in SG calculations a tight-binding band with $\rho(\epsilon) = 1/(\pi\sqrt{D^2 - \epsilon^2})$ are used, where D is the half-width of the band.

The tunneling between the molecular orbital and the leads is described by

$$H' = V_L(x)\hat{v}_L + V_R(x)\hat{v}_R, \quad (4)$$

and occurs via the hybridization operators (assuming here the tunneling is k -independent)

$$\hat{v}_{\alpha} = \sum_{k\sigma} c_{k\alpha\sigma}^{\dagger}d_{\sigma} + h.c. \quad (5)$$

multiplied by the displacement modulated overlap integrals

$$V_{\alpha}(x) \leftrightarrow V_{\alpha}(\hat{x}) \equiv V_{\alpha}(a + a^{\dagger}), \quad (6)$$

where the displacement is explicitly quantized. We find it convenient for symbol x to refer either to the operator $x \rightarrow \hat{x} = x = a + a^{\dagger}$, in the x - and second-quantized representations, respectively, or a real-valued expectation value for the displacement of the molecule. The precise meaning is clear from the context.

It is practical to define even and odd combinations of states in the leads, respectively

$$c_{ke(o)\sigma}^\dagger = \frac{1}{\sqrt{2}} \left(c_{kL\sigma}^\dagger \pm c_{kR\sigma}^\dagger \right). \quad (7)$$

In this basis H' reads

$$H' = V_e(x)\hat{v}_e + V_o(x)\hat{v}_o \quad (8)$$

where

$$V_{e,o}(x) = \frac{V_L(x) \pm V_R(x)}{\sqrt{2}}, \quad (9)$$

corresponding to tunneling to even and odd channel, respectively ($\hat{v}_{e,o}$ correspond to Eq. (5) for $\alpha = e, o$, respectively). Note that

$$|V_e(x)| > |V_o(x)| \quad (10)$$

if $V_{L,R}(x)$ are both positive or both negative for all x .

In this paper we perform the majority of calculations using the two functional forms of $V_\alpha(x)$ as follows.

A. Linear modulation (LM)

Expanded to lowest order in displacement the overlap integrals read

$$V_{L,R}(x) = V [1 \mp (gx + \zeta)], \quad (11)$$

where V sets the scale of the tunneling, $g \geq 0$ describes the strength of its modulation by displacement, and ζ characterizes the strength of the inversion symmetry breaking perturbation. In the symmetrized basis the overlap integrals take on the following form

$$V_e = \sqrt{2}V, \quad V_o = \sqrt{2}V(gx + \zeta). \quad (12)$$

Note that Eq. (12) does not satisfy the requirement Eq. (10) for $g|x|$ large enough.

B. Exponential modulation (EM)

Arguably more realistic is to model the modulation of tunneling by

$$V_{L,R}(x) = V [\exp(\mp gx) \mp \zeta], \quad (13)$$

or equivalently

$$V_e = \sqrt{2}V \cosh(gx), \quad V_o = \sqrt{2}V [\sinh(gx) + \zeta], \quad (14)$$

which are positive and satisfy the relation Eq. (10) manifestly. Clearly, by expanding the couplings to lowest order in x , the linearized version of the model is recovered.

Let us here define the magnitude of the bare hybridization Γ of the $g = 0$ models $\Gamma = \pi V_e^2 / (2D)$.

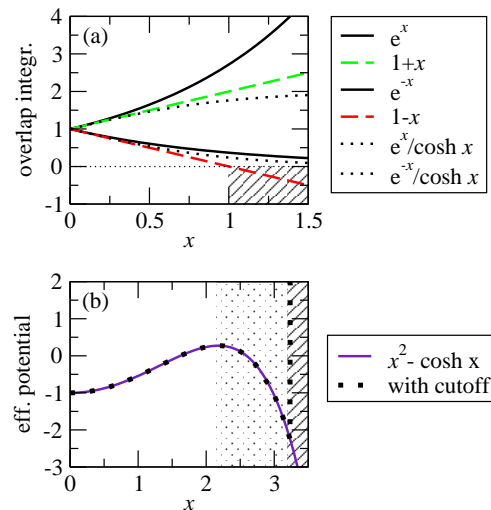


Figure 2: (Color online) (a) The breakdown of LM. The region where the amplitude of the linear approximation to overlap integral towards left lead starts to rise again for large enough x is indicated by dashed. (b) The breakdown of EM. In the right-hand part the effective potential drops without bounds. This is regularized by the phonon cutoff which corresponds to the hard-wall boundary. Two different cutoff regimes are indicated by dotted and dashed area.

C. Limitations of models

In LM, when $g|x| > 1$ one of the overlap integrals becomes negative and its absolute value starts to increase with increasing x which is an artifact of the linearization and does not occur in, *e.g.*, EM. For clarity of presentation, we plot the x -dependence of overlap integrals in Fig. 2(a) for LM (dashed), EM (full). The dashed area indicates the region where one of the overlap integrals changes sign.

On the other hand, the model with exponential dependence is unstable towards large displacements as can be understood by the following simple argument. For x large enough $V \exp(gx)$ and Ωx^2 are the largest energy scales in the problem. In this limit it suffices to consider only two sites coupled by a tunneling term with tunneling proportional to $\exp(gx)$. The total energy of one electron on these two sites $E \sim \Omega x^2 / 4 - V \exp(gx)$ is thus unbounded from below for large x . Therefore we anticipate the effective potential of this form, depicted in Fig. 2(b) (full), to be decreasing rapidly as a function of x in the right-hand part.

One solution of this problem is to add to the oscillator potential higher terms in displacement which corresponds to hardening of the 'spring' for large x . In our numerical calculations such a hardening is incorporated in the form of a phonon cutoff which acts as a hard-wall boundary, thereby eliminating the states corresponding to displacements larger than $\sim 2\sqrt{L}$, if L is the maximal number of allowed excited phonons. In Fig. 2(b) the dotted and

dashed region indicate two different cutoff regimes. For the larger cutoff also the resulting effective potential is plotted (dashed).

We can expect the results for EM to be strongly dependent on the cutoff because the choice of cutoff determines the form of the effective potential near *low* energies. Moreover, we find that EM for $L \rightarrow \infty$ is ill-defined: for example, according to the form of the effective potential we expect the average displacement (or its fluctuations for $\zeta = 0$) to diverge for each $g > 0$.

In this work we perform a comprehensive analysis of LM keeping in mind that the results for g large enough correspond to the unphysical regime where the inequality Eq. (10) is violated. Later we discuss also EM for a specific phonon cutoff to highlight which of the results of LM are generic (meaningful) for systems with displacement-modulated hybridization and which not. Alternatively, the exponential dependence of overlap integrals can also be regularized by renormalizing with a cosh function, Fig. 2(a) (dotted). We briefly discuss also such a model at the end of Section V.

III. NUMERICAL METHODS

Most of the numerical results presented here have been obtained using the well known Wilson's numerical renormalization group^{28,29}(NRG) method. NRG procedure is based on adding sites to the system iteratively with hopping to the n -th added site decreasing as $\Lambda^{-n/2}$. At each step the resulting Hamiltonian is diagonalized and lowest K eigenstates are kept. The exponentially decreasing hopping is essential to introduce all the energy scales while still keeping the numerical effort reasonable. Such a procedure is especially suitable for the Kondo problem where a range of energy scales contributes equally to the screening of the impurity spin. The algorithm is stopped after N_{\max} iterations. In the presented results we have typically used $\Lambda = 3 - 4$, $K = 2000$ (not counting the degeneracies due to spin, isospin, and parity symmetries³⁰ which have been explicitly taken into account) and $N_{\max} = 40$.

In order to gain additional insight and to make a relation with our previous work we compare the NRG results with the results obtained by the Schönhammer-Gunnarsson (SG)^{31,32} variational method. The details of our implementation of the variational method are given in our previous work^{20,33,34}. For reader's convenience we here just remark that it consists of finding the parameters of auxiliary noninteracting Hamiltonian \tilde{H} [of the same form as H in Eq. (1), but for $g = 0, U = 0$ and renormalized parameters $\tilde{V}_L, \tilde{V}_R, \tilde{\epsilon}$], which minimize the variational ground state energy $E = \langle \Psi | H | \Psi \rangle$, where the variational function Ψ is expressed in the basis of projection operators P_i acting on the Hartree-Fock ground state $|\Psi_0\rangle$ (which includes the phonon vacuum) of the

auxiliary Hamiltonian \tilde{H} ,

$$|\Psi\rangle = \sum_{ni} \psi_{ni} (a^\dagger)^n P_i |\Psi_0\rangle. \quad (15)$$

We have adapted the SG method also to extract the effective oscillator potential. This is obtained by restricting the parameters of the auxiliary Hamiltonian to yield $|\Psi_x\rangle$ for which the average $\langle \Psi_x | \hat{x} | \Psi_x \rangle = x$ is finite even for $\zeta = 0$. The dependence of the energy $\Delta E = \langle \Psi_x | H | \Psi_x \rangle$ on x constitutes our estimate of the effective oscillator potential. Technically, we use auxiliary parameter $\tilde{\zeta}$ to fix the asymmetry of \tilde{H} between hopping to left and right leads by expressing $\tilde{V}_{L,R} = (1 \pm \tilde{\zeta})\tilde{V}$ but still minimize the energy with respect to other parameters of \tilde{H} . Each $\tilde{\zeta}$ then leads to the effective potential defined by a particular pair of x and ΔE .

IV. ANALYTICAL RESULTS

Quantitatively the model Eq. (1) can be studied numerically and the results are presented in Section V. Nevertheless, by analytically deriving results in special limits we anticipate different regimes of behavior and the values of parameters where these regimes emerge.

A. Linear modulation

For U and Ω large it is sufficient to project the Hamiltonian on space consisting of states with singly occupied molecular orbital without excited phonons. By performing the Schrieffer-Wolff transformation described in Appendix B, the 2CK model is obtained with the antiferromagnetic coupling,

$$H_{2CK} = J_e \mathbf{S} \cdot \mathbf{s}_e + J_o \mathbf{S} \cdot \mathbf{s}_o, \quad (16)$$

between the spin on the dot \mathbf{S} and the spin densities \mathbf{s}_α in orbitals next to impurity in the even and odd channel, $\alpha = e, o$, respectively. The coupling constants are

$$J_e = 2V_e^2 \left(\frac{1}{-\epsilon} + \frac{1}{\epsilon + U} \right) \quad (17)$$

and

$$J_o = 2V_o^2 \left(\frac{1}{-\epsilon + \Omega} + \frac{1}{\epsilon + U + \Omega} \right). \quad (18)$$

The ratio

$$\frac{J_o}{J_e} = \frac{g^2}{1 + 2\Omega/U} \quad (19)$$

determines which of the channels dominates the screening. Let us use g_c to denote the value separating the small g regime, where the screening occurs in the even

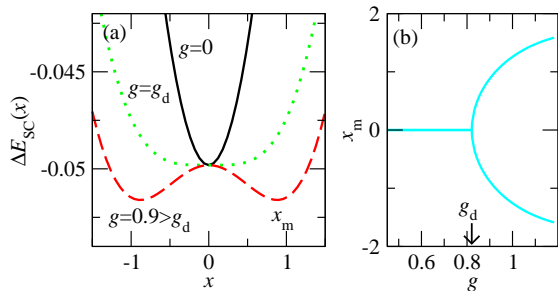


Figure 3: (Color online) Semi-classical estimate of the effective oscillator potential for LM. Parameters $\Omega = 0.1$, $\Gamma = 0.02$ are in units of D (half-width of the band).

channel, and large g regime, where the screening occurs in the odd channel. Hence for large U and Ω

$$g_c \sim \sqrt{1 + 2\Omega/U}. \quad (20)$$

The value $g = g_c$ corresponds to the unstable 2CK fixed point which separates the two (Fermi liquid) regimes.

In terms of the effective Hamiltonian, the $g < g_c$ ($g > g_c$) regimes corresponds to the state, where the hopping to left and right lead has equal and opposite phases, respectively. The non-Fermi liquid $g = g_c$ regime cannot be described in terms of (Fermi-liquid) effective Hamiltonian. Nevertheless, insisting upon this description, it can be regarded as a combination of states which correspond to two effective Hamiltonians in which left and right lead are respectively decoupled.

Turning now to the renormalization of the vibrational mode it is easy to demonstrate that the double well effective oscillator potential may form under the influence of a sufficient electron-phonon coupling $g > g_d$, where we define the delimiting value of the coupling constant. For $U = 0$ we can make a simple estimate on the form of the effective oscillator potential by a substitution $a \sim a^\dagger \sim x/2$, where x is a real-valued constant. In the wide-band limit (Γ/D small) the energy gain due to the hybridization is³⁵ $\Delta E_{\text{hyb}} = -2/\pi \tilde{\Gamma} \log D/\tilde{\Gamma}$, where we use the effective displacement-dependent hybridization $\tilde{\Gamma}(x) = \Gamma(1 + g^2 x^2)$. The elastic energy cost is $\Delta E_{\text{el}} = \Omega x^2/4$, hence in this semi-classical approximation the dependence of energy $\Delta E_{\text{SC}} = \Delta E_{\text{el}} + \Delta E_{\text{hyb}}$ on x can be written in a closed form

$$\Delta E_{\text{SC}}(x) = \Omega x^2/4 - (2/\pi) \tilde{\Gamma}(x) \log\{D/[\tilde{\Gamma}(x)]\}. \quad (21)$$

The prefactor of the x^2 -term in the small- x expansion is equal to $\Omega/4 - \{(2/\pi)g^2\Gamma[\log(D/\Gamma) - 1]\}$, hence for increasing g the elastic potential is softened and a double well effective potential emerges for g greater than g_d . We plot $\Delta E_{\text{SC}}(x)$ for few g in Fig. 3(a). From the estimate Eq. (21) the positions of the minima $|x| = x_m$ and g_d can

be extracted analytically,

$$g > g_d = \sqrt{\frac{\pi\Omega}{8\Gamma[\log(D/\Gamma) - 1]}}, \quad (22)$$

$$x_m = \sqrt{\frac{\pi\Omega(g - g_d)}{4\Gamma g_d^5}}. \quad (23)$$

We plot $x_m(g)$ in Fig. 3(b). In the following Section we compare x_m also to the numerical results of displacement fluctuations, which become enhanced for $g > g_d$ [see Fig. 4(a)].

In general, we expect $g_c > g_d$. Roughly speaking, the 2CK point occurs at g_c which is such that $1 - g_c|x| \sim 0$ should hold, so in the semi-classical estimate the double well-potential has to be preformed that its minima can occur at $x_m \gtrsim 1/g_c$. Because the double well potential evolves rapidly as a function of g (this assertion is later confirmed also by the SG results) the two values g_c and g_d are close [Fig. 4(a)].

In Table I we compare values of g_c calculated by the NRG simulation to Schrieffer-Wolff (SW) estimates and to estimates for the values of g_d obtained by the semi-classical estimate Eq. (22) or calculated numerically using SG method for few values of parameters. As expected, we find that the Schrieffer-Wolff estimate of g_c becomes more accurate for U, Ω large when the orbital is predominantly singly occupied and there are only few excited phonons. Conversely, the semi-classical estimate is more accurate for large number of excited phonons (small Ω) and small U but breaks down for large U . For example, for $\Omega = 1$ and $U = 3$ the value obtained by the semi-classical method (SC) overestimates g_d to the value which is larger than g_c obtained using NRG.

Based on the form of the effective potential, we anticipate that as g is increased the frequency ω of the oscillations decreases: the vibrational mode softens. After the two side-wells emerge, there are two types of oscillation, the high frequency part corresponds to the oscillations within each of the wells and the low frequency part to the slow tunneling between the degenerate minima (later we show numerically that after the soft mode emerges its frequency ω_0 decreases exponentially with g).

For $\zeta \neq 0$, we expect the left and right minimum of the effective potential to differ in energy. This energy difference, which is for small breakings proportional to ζ constitutes another characteristic energy and presents the lower limit on the frequency of the softened oscillations between the wells, as demonstrated later by numerical examples.

B. Exponential modulation

Let us perform the Schrieffer-Wolff transformation also on the model with exponential modulation of tunneling.

Table I: SC and SG: g_d obtained from semi-classical (SC) estimate and from SG simulations. SW and NRG: g_c calculated by SW estimates and from NRG simulations. SG method is inapplicable for very large U .

Ω	U	SC	SG	SW	NRG
0.1	0.3	0.82	0.85	1.29	0.84
0.1	0.6	0.82	/	1.15	0.85
1	0.03	2.60	2.59	8.22	3.11
1	0.3	2.60	2.32	2.76	2.32
1	3	2.60	/	1.29	1.28

We obtain

$$J_{e,o} = 2V^2 \sum_{m=0}^{\infty} \left(\frac{\delta_m^{e,o}}{-\epsilon + m\Omega} + \frac{\delta_m^{e,o}}{\epsilon + U + m\Omega} \right) \quad (24)$$

where $\delta_m^e = |\langle 0 | \cosh(gx) | m \rangle|^2$, $\delta_m^o = |\langle 0 | \sinh(gx) | m \rangle|^2$ which are both equal to $g^{2m} \exp(g^2)/m!$ for m even (odd) and zero for m odd (even), respectively. Note that $J_e > J_o$ for all values of parameters, hence no 2CK fixed point occurs in such a model. Note also that both J_α are exponentially dependent on g . The Kondo temperature, which is itself exponential in J , $T_K \propto \exp(-1/\rho J)$, is very sensitive to the value of g .

The effective potential which is unbounded from below for $L \rightarrow \infty$ is regularized by the phonon cutoff L . At fixed L we define $g_e(L)$ as g at which the molecule is attracted by the hard wall boundary as signaled by abrupt increase of displacements (shown later). Given L , the behavior of the model for $g > g_e(L)$ becomes dominated by the hard-wall boundary only. For instance, the full curve in Fig. 2(b) corresponds to a particular g which is smaller than g_e for the smaller phonon cutoff (dotted region) and larger than g_e for the larger phonon cutoff (dashed region). For $L \rightarrow \infty$, $g_e \rightarrow 0$.

V. NUMERICAL RESULTS

In this section we confirm by numerical examples the anticipations stated above. We first show the results for LM and then for EM. We treat separately the inversion symmetric $\zeta = 0$ and asymmetric $\zeta > 0$ cases. We use the half-width of the band D as the energy unit. Unless where explicitly stated, we take $U = 0.3$, $\Gamma = 0.02$, and $\Omega = 0.1$. All the results correspond to the particle-hole symmetric point, $\epsilon = -U/2$ and to the zero temperature limit.

A. Linearized model

1. Inversion symmetry: $\zeta = 0$

We begin by looking at the static quantities. The average displacement $\langle x \rangle$ for $\zeta = 0$ vanishes (as expected

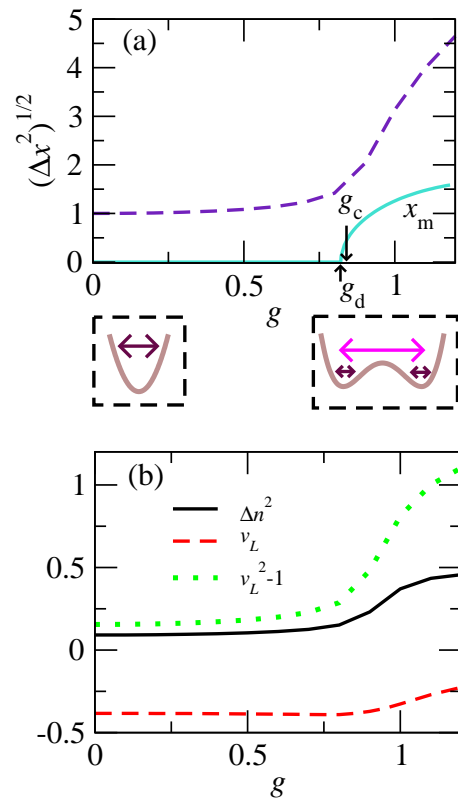


Figure 4: (Color online) (a) Fluctuations of displacement. (b) Fluctuations of charge, hopping to one of the leads and its fluctuations. The left (right) pictograms schematically present the effective oscillator potential before (after) the emergence of the soft mode. ($U = 0.3$, $\Gamma = 0.02$, $\Omega = 0.1$)

for an operator of odd parity under inversion in a state of well-defined parity). The fluctuations of displacement $(\Delta x^2)^{1/2} = \langle (x - \langle x \rangle)^2 \rangle^{1/2}$, shown in Fig. 4(a), increase monotonically with g . The slope of $(\Delta x^2)^{1/2}$ is increased considerably at $g \sim g_d$ ($\sim g_c$), where the double well like effective potential is formed, as indicated in pictograms. This change of slope is driven by the increased hybridization in the odd-channel. For comparison, we plot also the position of the minimum of the potential x_m (full line) obtained from the semiclassical estimate Eq. (21). It increases less rapidly than $(\Delta x^2)^{1/2}$ partially also because the wide-band assumption is not satisfied so strictly for large gx (large $\tilde{\Gamma}$).

In the $g > g_c$ regime also the fluctuations of charge $\Delta n^2 = \langle (n - 1)^2 \rangle$, shown in Fig. 4(b), are increased. However, the absolute value of the average of the hybridization operator $v_L = \langle \hat{v}_L \rangle$ is diminished, contrary to the naïve expectation. This is due to increasingly fluctuating sign of the overlap integral in this regime. On the other hand, the average of the hybridization operator squared $v_L^2 = \langle \hat{v}_L^2 \rangle$ is increased here, as expected.

In Fig. 5 we plot the effective oscillator potential $\Delta E(x)$ obtained by the procedure outlined in Section III. The dependence of ΔE on x is determined by the com-

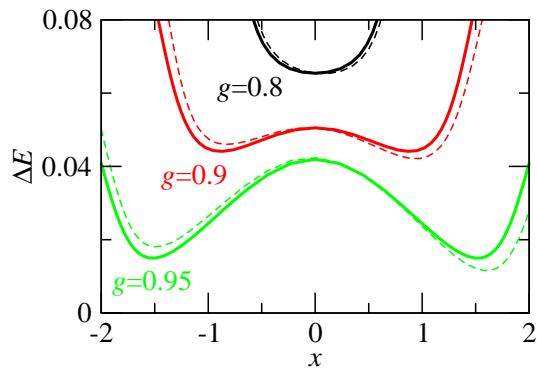


Figure 5: (Color online) The evolution from single well to double well effective oscillator potential calculated by the SG method. Inversion symmetric $\zeta = 0$ (full) and perturbed $\zeta = 0.01$ (dashed) cases are shown. Other parameters as in Fig. 4.

petition between the kinetic energy gain and the cost in the oscillator potential. For g large enough the double well structure is formed. The level of the asymmetry of ΔE is determined by the value of ζ .

In Fig. 6 we plot the NRG flow diagram: the energies of the lowest few eigenstates in units of characteristic energy of a particular iteration $\omega_N \propto \Lambda^{-(N-1)/2}$ as the function of the NRG iteration number N . The fingerprint of the Fermi liquid ground state are the equidistant low-lying quasi-particle excitations³⁶ which are seen in Fig. 9 for large N , irrespective of g . By comparing the top two panels with the bottom panel it is seen, that the roles of even and odd parity states are interchanged in the Fermi-liquid regime (right-hand side of each panel) corresponding to the change of the screening channel. The value of g at which this change occurs is the NRG estimate of g_c .

For $g \sim g_c$ (bottom panels) the unstable 2CK fixed point is discerned at intermediate N (~ 20 for the plotted case) where the eigen-energies are almost N -independent. Here, the ratios of eigen-energies are proportional to the predictions of the conformal field theory³⁶ $(0, 1/8, 1/2, 5/8, 1, 9/8, \dots)$ (horizontal bars), and cannot be related to excitations of quasi-particles. At increasingly lower energy scales (at increasingly large N) for g increasingly close to g_c the asymmetry of the coupling to the channels which is a relevant perturbation drives the flow towards the (stable) Fermi liquid fixed point.

Now we turn to the renormalization of the phonon propagator by the electron-phonon coupling. The dynamical information about oscillator is contained in the displacement Green's function. The displacement spectral function

$$\begin{aligned} \mathcal{A}(\omega) &= -\frac{1}{\pi} \text{Im} \ll x, x \gg_{\omega} = \\ &= -\frac{1}{\pi} \text{Im} \int_0^{\infty} (-i) \langle [x(t), x(0)] \rangle e^{i\omega t} dt \end{aligned} \quad (25)$$

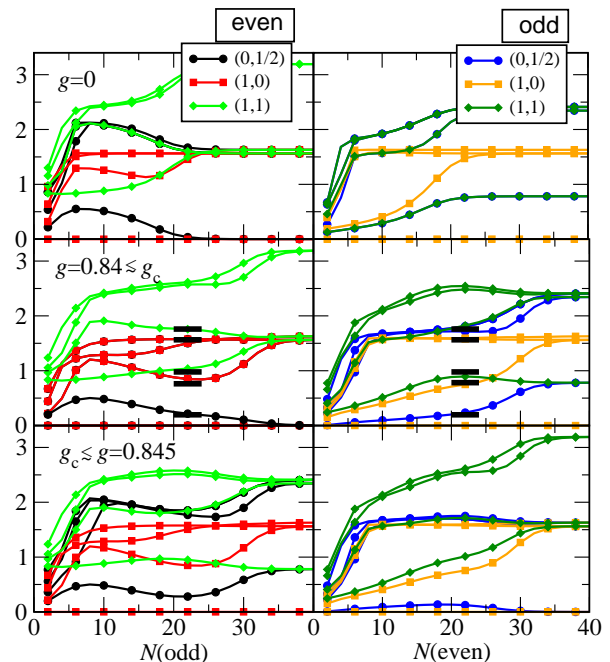


Figure 6: (Color online) NRG flow diagram. In the left (right) panels eigen-energies of states of even (odd) parity are shown for odd (even) number of NRG iterations, respectively. The states are labeled by (Q,S) : total charge Q and total spin S quantum numbers. The thick horizontal bars are the conformal field theory predictions for 2CK fixed point. Parameters are as in Fig. 4.

is an odd function of ω due to the hermiticity of x (unlike $\text{Im} \ll a, a^\dagger \gg_{\omega}$ which is odd only for the inversion symmetric case $\zeta = 0$). Since $\mathcal{A}(\omega)$ is in NRG evaluated for a finite system it consists of several δ -peaks of different weights. To obtain a smooth spectral function we have used the Gaussian broadening on the logarithmic scale³⁷, where the Dirac δ function is broadened according to

$$\delta(\omega - \omega_n) \rightarrow \frac{1}{b\omega_n\pi} \exp \left\{ - \left[\frac{\log(\omega/\omega_n)}{b} \right]^2 - \frac{b^2}{4} \right\}, \quad (26)$$

and we used $b = 0.3$ in our calculations.

In Fig. 7(a) we plot $\mathcal{A}(\omega)$ for various g . The width of the high frequency peaks is overestimated (the extreme example is the $g = 0$ peak at Ω for which the width should vanish) due to the broadening procedure described above. We could use Dyson equation^{38,39} to obtain sharper peaks but on one hand there is no *a priori* guarantee that such a procedure gives more accurate results for large g and on the other hand we do not use the width of the peaks as a means to draw any quantitative conclusion.

For intermediate g [starting at $g \sim 0.5$ for the parameters used in Fig. 7(a)] the vibrational mode begins to soften: the peak moves to lower frequencies. At still larger g (at value near $g \sim g_c$) two peaks emerge. Characteristic dependence of $\mathcal{A}(\omega)$ in this regime is schemat-

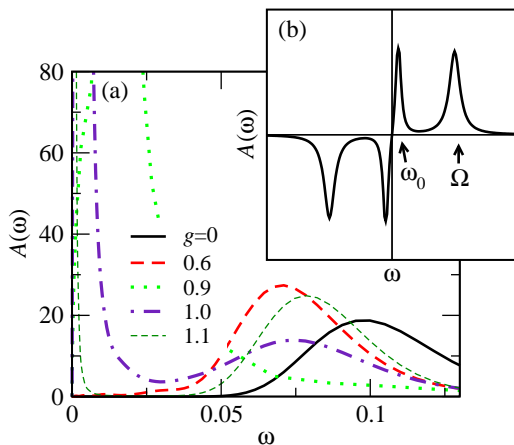


Figure 7: (Color online) (a) Displacement spectral functions for various g . Note the softening of the phonon mode. For large g only small amount of spectral weight resides at low frequencies. The peaks at large frequencies appear broader than they should be because of the broadening procedure described in the text. Parameters are as in Fig. 4. (b) Spectral function after the emergence of the soft mode schematically. The frequencies of the soft mode ω_0 and the high-frequency oscillation at $\omega \sim \Omega$ are indicated.

ically presented in Fig. 7(b). The frequency ω_0 and the weight of the low frequency peak decrease with increasing g . This behavior is understood in terms of the effective oscillator potential (Fig. 5, pictograms in Fig. 4). For g small, the potential is only weakly distorted from the bare oscillator potential. For intermediate g the double well potential starts to emerge. For large g the double well potential is already well established and the major part of the spectral weight corresponds to the oscillations within each of the wells. The minor, low frequency part corresponds to increasingly slow tunneling (see also Fig. 10) between the degenerate minima of the potential.

The inversion symmetry enables one to calculate the conductance using the scattering phase shifts as described in Appendix C. Except possibly at the isolated point $g = g_c$ the conductance evaluated by Eq. (C8) is unity²¹ because the scattering phase-shifts in the even and odd channel are $\pi/2(0)$ and $0(\pi/2)$, for $g < g_c$ ($g > g_c$), respectively and the rotation angle $\theta = \pm\pi/4$.

2. Broken inversion symmetry: $\zeta > 0$

It is impossible to experimentally produce perfectly symmetric devices, therefore it is interesting to check for the influence of the inversion symmetry breaking term of relative strength ζ . We plot static correlations for $\zeta = 0.01$ in Fig. 8. The absence of inversion symmetry is reflected in the average displacement which is nonzero and monotonically increases with increasing g . As in the case with $\zeta = 0$ the average of x^2 starts to rise considerably at $g \sim g_c$. However, at still larger g the av-

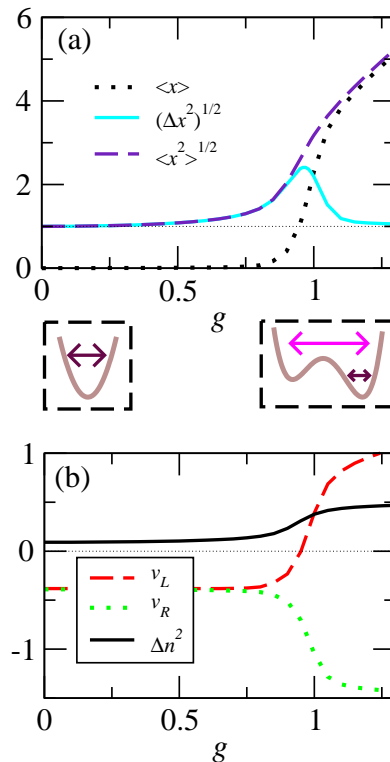


Figure 8: (Color online) Static quantities for system with broken inversion symmetry. (a) Averages of x , x^2 , and Δx^2 . (b) Averages of hopping v_L and v_R and fluctuations of charge. The breaking of inversion symmetry $\zeta = 0.01$. Other parameters as in Fig. 4.

erage displacement also starts to rise. Let us by g_{AS} denote the value of g where the fluctuations of displacement $\Delta x^2 = \langle (x - \langle x \rangle)^2 \rangle$ are maximal. For $g > g_{AS}$ the ground state is strongly asymmetric with increased average displacement.

The fluctuations of charge are similar to the $\zeta = 0$ case. Expectation values of v_L and v_R now differ and one of them changes sign for large enough $g \gtrsim g_{AS}$ (without impact to the rest of the physics).

The finite size spectra (not shown here) are that of the Fermi liquid; the occurrence of the non-Fermi liquid fixed point is inhibited by the breaking of inversion symmetry.

When compared to the $\zeta = 0$ case (Fig. 7) the spectral functions (Fig. 9) for $g \lesssim g_{AS}$ are alike while for the $g \gtrsim g_{AS}$ the frequency of the soft mode oscillation ω_0 saturates and does not fall to zero. This is more clearly seen in Fig. 10 where we plot the position of the low-frequency peak for both ζ as a function of g . The weight of the low frequency peak at ω_0 diminishes for $\zeta = 0$ exponentially with increasing g .

We plot $\mathcal{A}(\omega)$ for different ζ and fixed $g = 1.05 > g_{AS}$ in Fig. 11. The characteristic frequency of the soft mode now corresponds to the difference between the energies in both minima which is proportional to ζ as shown in the inset of Fig. 11.

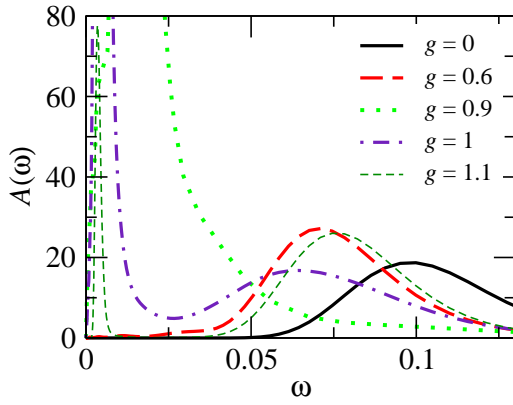


Figure 9: (Color online) Displacement spectral functions for various g , $\zeta = 0.01$. Other parameters as in Fig. 4.

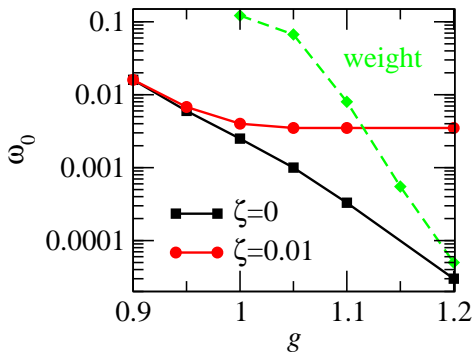


Figure 10: (Color online) The frequency (full lines) of the soft mode peak as a function of g . The weight of the soft mode peak for $\zeta = 0.01$ and normalized to some arbitrary value (dashed). Other parameters are as in Fig. 4.

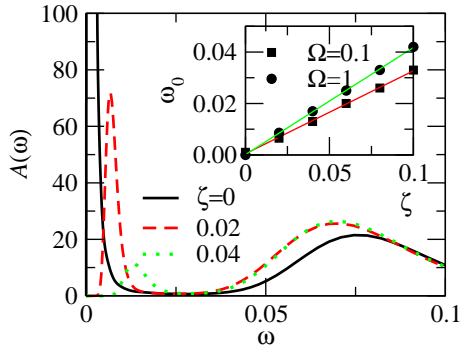


Figure 11: (Color online) (a) Displacement spectral functions for fixed $g = 1.05$ and $\zeta = 0, 0.02, 0.04$. Note the reduction of weight of low frequency peak on increasing ζ . The high energy peak of $\zeta = 0$ case is approached at still smaller ζ . Inset: The position of low frequency peak as a function of ζ for $\Omega = 0.1$, $g = 1.05$ and $\Omega = 1$, $g = 7$. The full lines are fits to the data with slopes 0.32 and 0.42 for $\Omega = 0.1, 1$, respectively. The position of the peak is not dependent on g , when g is large enough. Other parameters are as in Fig. 4.

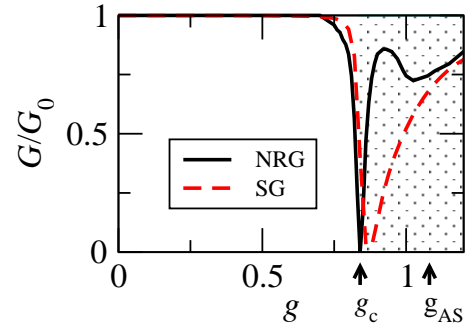


Figure 12: (Color online) Conductance as calculated from the current-current correlation function obtained by NRG (full) and from the SG method. The shaded region indicates the region the results are outside of the scope of the linearized model. $\zeta = 0.01$, other parameters are as in Fig. 4.

Such behavior is easily understood in terms of the effective potential pictorially shown in Fig. 8. For small to intermediate g the soft mode begins to emerge as the shape of the potential is transformed to a double-well like form. For positive ζ the right well is lower in energy than the left well by energy $\Delta \propto \zeta$. When on increasing g further the characteristic frequency of the tunneling between the wells decreases below Δ the tunneling is suppressed. The major part of the displacement spectral weight is in this regime due to the tunneling within the lower of the wells. The average displacement increases, its fluctuations approach unity. Note that even a minor breaking of inversion symmetry results in a strongly asymmetric state through the mechanism described here.

The conductance for $\zeta > 0$ cannot be obtained from the scattering phase shift alone since the rotation angle θ (see Appendix C) is not known in the present case of broken symmetry. Therefore we calculated the conductance from the current-current correlation function. We plot the conductance calculated by NRG and SG in Fig. 12. The conductance decreases at $g \sim g_c$ to zero. This minimum corresponds to the virtual decoupling of the left lead, $1 - gx \sim 0$, there on the average. In the NRG data, another minimum occurs at $g \sim g_{AS}$ where the average displacement starts to grow, a feature which the effective Hamiltonian of the SG method fails to capture. However, we remark that the discrepancy is especially visible for the parameters used here for which $g_c \sim g_{AS}$ (compare also with data given in Appendix A). The results of NRG and SG for $g > g_{AS}$ agree again. Here the fluctuations of displacement are diminished and the behavior is efficiently described in terms of the effective Hamiltonian with asymmetric coupling to the leads.

As remarked already in the discussion where the models have been introduced the region of parameter space $g \gtrsim g_c$ (shaded) lies outside the scope of LM. The increase of the conductance after its complete suppression at $g \sim g_c$ is due to the overlap with the negative amplitude when states for which $1 \pm gx < 0$ contribute consid-

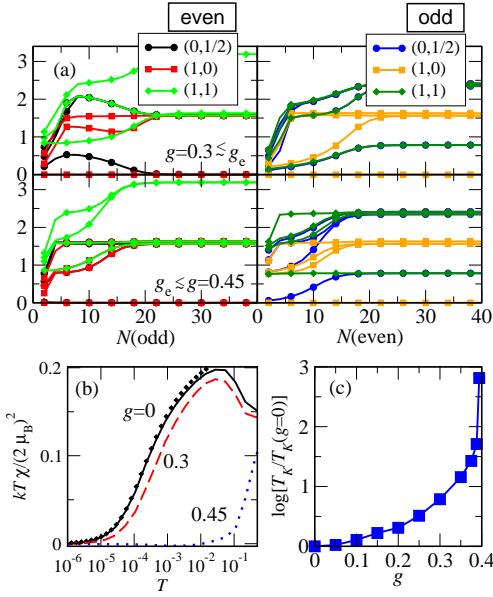


Figure 13: (Color online) Model with exponential modulation of overlap integrals (EM). $L = 10$, other parameters as in Fig. 4. (a) NRG eigenvalues. (b) Impurity contribution to magnetic susceptibility. For $g > g_e$ the local moment regime is absent. Kondo model. Diamonds indicate the susceptibility calculated using the Bethe ansatz. (c) The Kondo temperature.

erably to the transport. The access to this region is probably unaccomplishable in the experiments with transport through molecules.

B. Exponential model

We now turn to the model with exponential modulation. As noted before here even for the inversion symmetric model ($\zeta = 0$) the 2CK Kondo fixed point is inaccessible because the coupling to the even channel is invariably stronger compared to the coupling to the odd channel. This is reflected also in the finite size spectra shown in Fig. 13(a) which always correspond to a Fermi liquid ground state with the spin screened by the even conduction channel. Such behavior is expected also of the experimentally realized molecular junctions. The even and the odd channels do not inter-change their roles in the screening process by increasing g confirming that such an inter-change in LM is indeed an artifact of the linearization.

In Figs. 13(b) we plot the impurity contribution to the magnetic susceptibility χ . Dimensionless susceptibility $kT\chi/(2\mu_B)^2$, where k is the Boltzmann constant and μ_B the Bohr magneton, has a peak at intermediate temperatures corresponding to the local moment regime provided that $g < g_e$. For $g > g_e$ the local moment regime is absent. By fitting the Bethe ansatz results for $S = 1/2$ Kondo impurity to the numerically calculated suscepti-

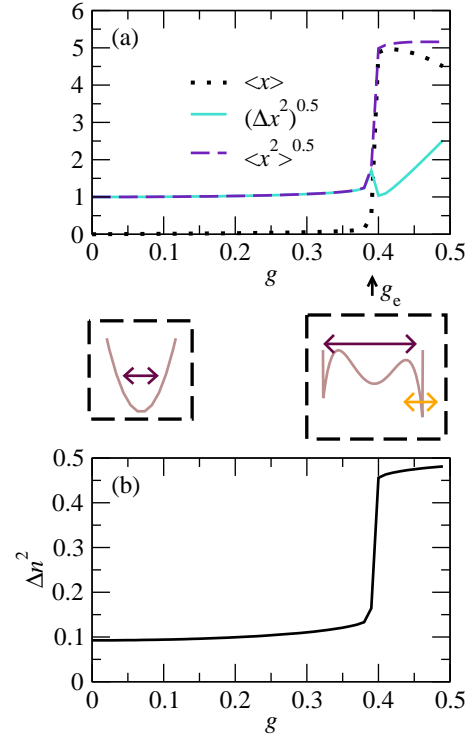


Figure 14: (Color online) (a) Average displacement and its fluctuations. (b) Fluctuations of charge. Phonon cutoff $L = 10$, $\zeta = 0.1$, other parameters as in Fig. 4.

bility, following the procedure described in Refs. 40,41,42, we obtain the estimate of the Kondo temperature T_K which we plot in Fig. 13(c). T_K is increasing rapidly near g_e as effective $U/\Gamma \rightarrow 0$ there. For $g > g_e$ the Kondo temperature is not defined because there is no local moment in the system.

In Fig. 14(a) we plot the expectation values of displacement and its fluctuations for $\zeta = 0.1$. For $g > g_e \propto \log \Omega \times \text{const}(L)$, the displacement rises abruptly to the values which are limited only by the phonon cutoff; for $\zeta = 0$ (not shown) the same applies to the fluctuations of displacement (displacement is zero). The abrupt increase is due to the increased hybridization which is exponential in displacement. The gain in the kinetic energy is uncompensated by the cost in oscillator potential which is only quadratic in the displacement operators. In this regime, due to the exponentially increased hybridization, the fluctuations of charge, shown in Fig. 14(b), are near-maximal, the molecule effectively 'sticks' to one of the leads in the effective potential presented in the right pictogram which has the same form as the function plotted in Fig. 2(b) (dashed).

The value g_e can be estimated by first recognizing that the maximum x is bounded by the phonon cutoff L : $x \lesssim x_{\text{max}} = 2\sqrt{L}$ and then solving $\Omega x_{\text{max}}^2/4 = V \exp(gx_{\text{max}})$

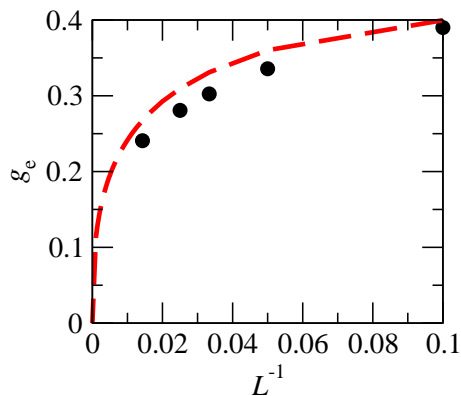


Figure 15: (Color online) Values g_e where the breakdown of the exponential model occurs for phonon cutoffs $L = 10, 20, 30, 40, 70$ (circles). Other parameters are as in Fig. 4. Semi-classical estimate of g_e (dashed).

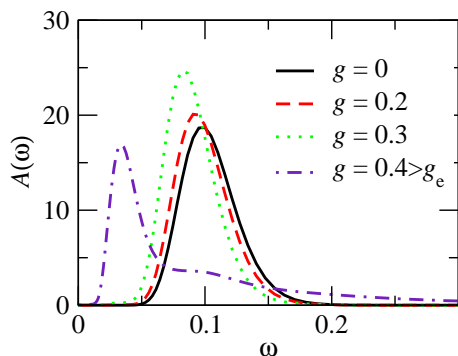


Figure 16: (Color online) Spectral functions exponential modulation. $\zeta = 0.1$, $L = 10$, other parameters as in Fig. 4.

for g , which gives

$$g_e = \frac{1}{2\sqrt{L}} \log \left(\frac{\Omega}{V} L \right). \quad (27)$$

The comparison between this estimate and the numerical data is shown in Fig. 15. In the limit $L \rightarrow \infty$ $g_e \rightarrow 0$. The important result of this analysis is that the model with exponential modulation of hybridization is not well-defined with quadratic stabilizing potential only; the results are dependent on (moreover, defined by) the cutoff.

In Fig. 16 we plot the spectral function $\mathcal{A}(\omega)$. With increasing $g \lesssim g_e$ the bare oscillator peak starts to soften. At $g > g_e$ the molecule is attracted next to the hard wall boundary and remains mainly trapped into one of the wells defined by the phonon-cutoff. The high frequency part of the spectral function in Fig. 16 corresponds to the oscillations within these wells. The wells are strongly anharmonic which is reflected in the broad distribution of spectral weight. The low frequency part of the spectral weight is due to the oscillations between the wells.

A natural question which arises at this point is whether

it is possible to tune the parameters so as to drive EM to the regime with developed double well potential, but for g sufficiently lower than g_e , so that the wells are not next to the hard wall boundary. For the parameter set used in the results shown, for example, this is not possible, because

$$g_d > g_e \quad (28)$$

for all L . We show below that inequality Eq. (28) holds generally.

We begin by maximizing g_e with respect to L (treating L as if it was a continuous variable) and obtain

$$g'_e = \max_L g_e(L) = \frac{\pi^{1/4} \sqrt{\Omega}}{e(D\Gamma)^{1/4}}. \quad (29)$$

The ratio between g_d defined in Eq. (23) and g'_e can now be evaluated. We obtain that $g_d/g'_e \geq (e^7 \pi)^{1/4}/4 \sim 1.92$. The double well potential develops in EM also for g_e , but the wells are near the boundary defined by the phonon cutoff.

As a side note we remark here that we investigated also the behavior of a model in which the couplings to the left and right leads are proportional to $\exp(\mp gx)/\cosh(gx)$, respectively [the coupling to the even channel is here constant and the coupling to the odd channel is proportional to $\tanh(gx)$]. The overlap integrals in this model satisfy the inequality Eq. (10) and the normalization with the cosh function eliminates the diverging behavior for large x .

For this model we evaluated the matrix elements of the Hamiltonian $\langle m|H|n\rangle$ ($|m\rangle, |n\rangle$ correspond to states with m, n excited phonons) in the real space by reintroducing the Hermite polynomials which is numerically more stable than the expansion of $\tanh(gx)$ in the power-series in $x = a + a^\dagger$ [in the case of EM discussed earlier we evaluated $\langle m|\exp(gx)|n\rangle$ analytically via the Baker-Hausdorff equality].

Due to weaker dependence of the overlap integrals on displacement the effects of the electron-phonon coupling in this model are less pronounced. The displacement and its fluctuations which we plot in Fig. 17(a) are close to 0 and 1, respectively, for the same parameter set as used before. This is accompanied by only minor softening of the phonon mode, as shown in Fig. 17(c). The fluctuations of charge and the expectation values of hopping, plotted in Fig. 17(b) are likewise only minorly distorted from the $g = 0$ case. Note that we used $\zeta = 0.1$ here, therefore the hoppings towards left and right leads differ considerably already for the $g = 0$ case, a feature which is only slightly (compared to LM and EM) amplified by the dependence of the overlap integrals on x for $g > 0$. The reason for this moderate dependence of quantities on g is that the largest energy the system can gain by increasing the displacement is of the order of $V \propto \sqrt{\Gamma}$, which is comparable to the elastic energy Ωx^2 already for the displacements of order 1. Note that we used $\Omega = 0.1$, for smaller Ω , *i.e.*, softer 'spring' the effect of the electron-phonon coupling could be larger. Finally, let us remark

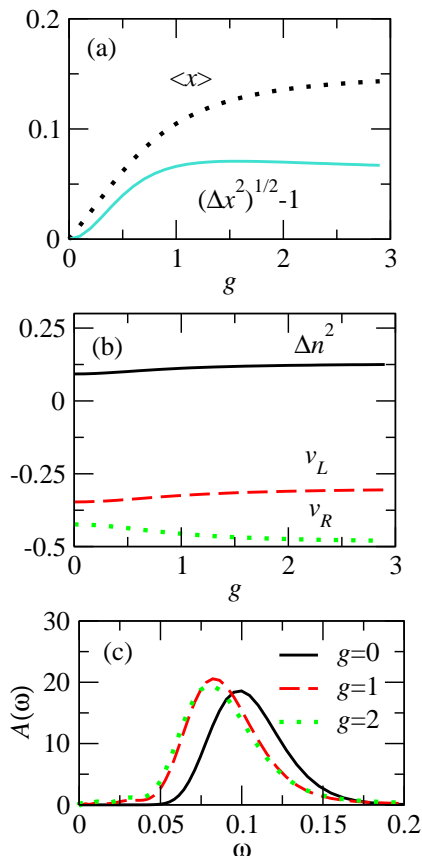


Figure 17: (Color online) Results for model with overlap integrals modulated as $V_{L,R}(x) \propto \exp(\mp gx)/\cosh(gx)$, respectively. (a) Displacement and its fluctuations. (b) Expectation values of hoppings and fluctuations of charge. (c) Displacement spectral function. $\zeta = 0.1$, other parameters as in Fig. 4.

that similarly to EM no change of the symmetry of the screening channel occurs here for $\zeta = 0$.

VI. CONCLUSION

In summary, we analyzed a molecule oscillating between two electrodes. The overlaps between the molecular orbital and the orbitals in the leads are determined by the position of the molecule x . To model this situation we used two generic types of the dependence of the overlap integrals on x : linearized and exponential.

We find that the inversion symmetric linearized model has a 2CK critical point at some critical coupling $g = g_c$ which separates the regimes of spin screened by the channels of different parity. Simultaneously, by increasing the electron-phonon coupling the phonon mode softens. At $g \gtrsim g_c$ the phonon propagator develops two peaks, one softens and one hardens on increasing g . This is consistent with the picture of a double well effective oscillator potential. The soft mode corresponds to the slow tunneling between the degenerate minima and the high-

frequency mode to the oscillations within each of the wells. The frequency and the weight of the soft mode peak diminish exponentially on increasing g .

Inclusion of the explicit breaking of the inversion symmetry on the one hand removes the degeneracy between the two scattering channels and hence inhibits the 2CK fixed point. The sharp transition between the two Fermi liquid states via a non Fermi liquid state is now replaced by a continuous rotation of the screening state in the channel space from an almost symmetric to an almost antisymmetric linear combination of the left and right states. This continuous rotation is accompanied by the dip in conductance near the point where one of the leads is decoupled. Average fluctuations of displacement (and consequently, due to the increased hybridization, charge) start to increase more rapidly for $g \gtrsim g_c$.

On the other hand, for g larger still, when the characteristic frequency of the soft modes approaches the energy of the breaking, the average displacement starts to increase significantly and its fluctuations diminish: the oscillator predominantly oscillates in one of the two wells of the effective potential in this regime. Through the softening only a minor breaking of inversion symmetry can result in a significantly asymmetric configuration (which could, at least partially, also account for the strongly asymmetric configurations observed in experiments). The characteristic frequency of the soft mode does not diminish on increasing g below the value which is set by the magnitude of the breaking ζ .

In the linearized model, the competition between screening in the channels of different parity arises because the coupling to the symmetric channel is taken constant while the coupling to the odd channel is proportional to gx which overcomes the symmetric one for sufficiently large g . This is, however, an artifact of the linearization. In the original model (Fig. 1) the magnitude of the ratio between the coupling to the even and odd channels is proportional to $|[V_L(x) + V_R(-x)]/[V_L(x) - V_R(-x)]|$, which is always greater than 1 as long as all the overlap integrals have equal sign. The change in the sign of the overlap integrals in the effective models is reflected also in the change of the sign of the expectation values of $v_{L,R}$ in the linearized model with the broken inversion symmetry.

As an example of the more general model, in which this arguably unphysical feature is absent, we tested the model with exponential modulation of overlap integrals. As predicted from the arguments given above, no traces of the 2CK fixed point are seen in the finite-size spectra here. On the other hand, the exponential increase of hybridization has as a consequence the exponential gain in the kinetic energy, hence this model is not stable against large distortions as the stabilizing oscillator potential is only quadratic in displacement. The value of g at which this instability starts is set by the phonon cutoff. This is because the largest displacement is bounded by the cutoff $x \sim 2\sqrt{L}$ and for each g the cost in the elastic energy might not yet be overcome at this cutoff (but would be

if the calculations were performed at larger cutoff). Nevertheless, by restricting our attention to the calculations for a definite cutoff, we find that for small g the softening occurs and for large g , the molecule is found localized next to the boundary defined by the phonon cutoff.

In analyzed models, generally the electron-phonon coupling softens the elastic force which confines the oscillator to the central position between the electrodes, therefore even small perturbations which break the inversion symmetry can significantly enhance the average displacement from the center of inversion and suppress the conductance. It should be noted also that both models give rise to spurious results for large g and should be applied to the experimental situation with care. In particular, model with exponential modulation is good-defined only at $g < g_e$ where $g_e(L)$ is a decreasing function and $g_e \rightarrow 0$ as $L \rightarrow \infty$.

Another possible implications of the present work for the experiment, although not discussed at length here is the enhancement of the Kondo temperature. It is likely that the tunneling to the electrodes is exponentially dependent on the position of the molecule, therefore already for small electron phonon coupling constant, the Kondo temperature can be significantly increased. For the gate voltage affects the behavior of the models discussed here in a way dissimilar to the conventional Anderson model, these might also account naturally for the anomalous dependence of the Kondo temperature on the gate-voltage.

Let us also comment on the relevance of the presented work outside the scope of the experiments with molecular conductors. In recent years, considerable advance in the understanding of strongly correlated electron systems has been achieved within the dynamical mean field theory⁴³ and its extensions to cluster dynamical field theory. In this theory bulk correlated electron systems are solved by mapping onto impurity problems. Likewise, bulk systems with electron-phonon coupling are mapped onto impurity (or impurity-cluster) problems with coupling to phonons. In this regard the knowledge of the behavior of the impurity problems is a convenient guide in the interpretation of the DMFT results. The results obtained in this work for the linearized model correspond to the general two-band case where the coupling to one of the bands is phonon-assisted. The large g regime which we dismissed as unphysical could prove relevant in this context.

Our results could also be applied to the studies of nanoelectromechanical systems^{44,45,46,47,48} (NEMS). In NEMS the tunneling to electrodes is modulated by the displacement of the cantilever in a similar fashion as analyzed in this work. Once the dimensions of these devices are reduced to such an extent that the frequencies of the oscillations will become comparable to other scales, such as the bias at which the devices are operated, softening of the vibrational mode and susceptibility towards large displacements could be observed. For instance, we predict the frequency of the oscillations will diminish if the tunneling rate from the electrodes to the perpendicularly

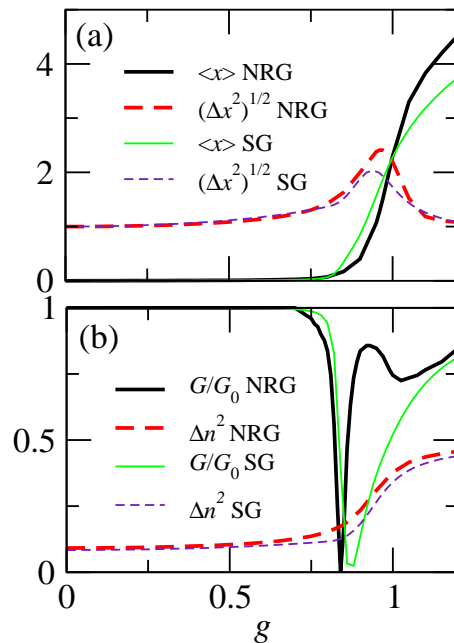


Figure 18: (Color online) Comparison between Shönhammer-Gunnarsson and NRG results. (a) Displacement and displacement fluctuations. (b) Conductance and charge fluctuations. $U = 0.3$, $\Gamma = 0.02$, $\Omega = 0.1$, $\zeta = 0.01$.

situated cantilever immersed between them is increased.

Acknowledgments

We are indebted to P. Prelovšek for a remark which partially inspired this work. We acknowledge discussions with R. Žitko and the use of his implementation of NRG (<http://nrgljubljana.ijs.si>) as-well as discussions with T. Rejec and his contributions in the development of the SG code. The work is supported by Slovenian Research Agency (SRA) under grant P1-0044.

Appendix A: COMPARISON TO SCHÖNHAMMER-GUNNARSSON PROJECTION-OPERATOR METHOD

In this appendix we compare the results of NRG calculations to the results obtained by the SG method. Let us summarize first the results we have obtained using the SG method for model II of Refs. 18,21. We have found that for g large enough the variational solution with broken inversion symmetry is lower in energy. This occurs even for $\zeta = 0$ when the inversion symmetry should persist. That indicates that for large g due to the instability in the system the SG method fails giving a solution with 'spontaneously' broken symmetry. Such failure is typical of the mean-field treatment. However, it was not clear

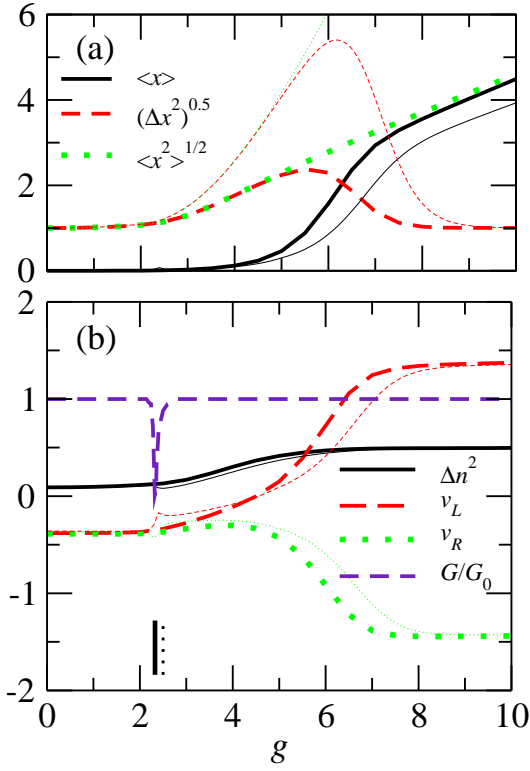


Figure 19: (Color online) $\Omega = 1$, other data as in Fig. 18. Thick lines: NRG, thin lines: SG; (a) Expectation values of x and its fluctuations. (b) Fluctuations of occupancy and expectation values of hoppings to left and right leads. The vertical lines denote g_c (thick) and the value of g where the minimum of conductance calculated by SG method occurs (dotted). Conductance curves (dashed) obtained by NRG and SG coincide.

whether the failure occurs at the point where the symmetry of the screening channel is changed or at the point when the soft mode is formed (or the two phenomena occur simultaneously).

In Fig. 18 we compare the displacement, its fluctuations and the fluctuations of charge calculated by SG method to the NRG results. They match closely, with the exception of discrepancies in the precise values of increased displacement fluctuations and range of g where these occur. Conductance is discussed in the main text, here we re-plot the curve for completeness.

In Fig. 19(a) we show the results for $\Omega = 1$ where the discrepancy between NRG results (thick) and SG results (thin) is larger. In this regime SG method overestimates the value of displacement and its fluctuations. More interestingly, in Fig. 19 (b) the jump in expectation values of hopping operators is seen in the variational results near the value where the change of the symmetry of the screening channel occurs. Here also a small peak in displacement [Fig. 19(a), difficult to discern] and minimum of conductance occur.

If $\zeta = 0$ there is no 'spontaneous' symmetry breaking

in SG method for this Ω . By combining these results we conclude that the appearance of asymmetric solution in SG will coincide with the change in the symmetry of the screening channel from even to odd, but only when the soft mode is sufficiently developed, otherwise only a finite jump in v_L , v_R occurs there.

Appendix B: SCHRIEFFER-WOLFF TRANSFORMATION

To obtain the effective-low energy Hamiltonian H_{eff} we first divide the Hamiltonian into two parts⁴⁹

$$H = H_0 + \lambda H' \quad (\text{B1})$$

where H_0 , which for our example reads

$$H_0 = \epsilon n + U n_\uparrow n_\downarrow + \Omega a^\dagger a + H_L + H_R, \quad (\text{B2})$$

is diagonal in the low ($n = 1$, no excited phonons) and high ($n = 2, 0$, with excited phonons) energy subspaces (for $\epsilon \sim -U/2$, U and Ω large). The hybridization part

$$H' = V v_e + V g x v_o \quad (\text{B3})$$

provides the mixing between the low and high energy subspaces and λ serves as an expansion parameter to be set to 1 at the end of the derivation.

Then a canonical transformation generated by some unitary operator $e^{\mathcal{S}}$ is performed to obtain the block-diagonal

$$\tilde{H} = e^{\mathcal{S}} H e^{-\mathcal{S}} = \begin{pmatrix} H_L & 0 \\ 0 & H_H \end{pmatrix}. \quad (\text{B4})$$

By expanding Eq. (B4) in terms of nested commutators $\tilde{H} = H + [\mathcal{S}, H] + [\mathcal{S}, [\mathcal{S}, H]]/2 + \dots$ and the generator \mathcal{S} as a power-series in λ , $\mathcal{S} = \mathcal{S}_1 \lambda + \mathcal{S}_2 \lambda^2 + \dots$, to second order in λ the following should hold:

$$\begin{aligned} \tilde{H} = H_0 + \lambda(H' + [\mathcal{S}_1, H_0]) + \\ + \lambda^2([\mathcal{S}_1, H'] + \frac{1}{2}[\mathcal{S}_1, [\mathcal{S}_1, H_0]] + [\mathcal{S}_2, H_0]). \end{aligned} \quad (\text{B5})$$

Relation Eq. (B5) is satisfied to lowest order in λ by demanding

$$H' + [\mathcal{S}_1, H_0] = 0. \quad (\text{B6})$$

Since \mathcal{S}_1 can be chosen completely block-off-diagonal the commutator $[\mathcal{S}_1, H']$ is block-diagonal, therefore Eq. (B4) is satisfied also to second order in λ by taking $\mathcal{S}_2 = 0$. Looking now at the matrix element of Eq. (B6) in the basis of eigenstates of H_0 (we will use Latin indices for states in low-, and Greek indices for states in high-energy subspaces), we obtain $\mathcal{S}_{\alpha b} = H'_{\alpha b}/(E_\alpha - E_b)$.

Finally, the high energy part is neglected by projecting to the low energy subspace

$$H_{\text{eff}} = P_{\text{low}} H_0 P_{\text{low}} + H_{\text{eff}}^{\text{I}} \quad (\text{B7})$$

with the projector

$$P_{\text{low}} = |0\rangle\langle 0| [n_{\uparrow}(1 - n_{\downarrow}) + n_{\downarrow}(1 - n_{\uparrow})] \quad (\text{B8})$$

where $|m\rangle$ denotes normalized state with m excited phonons and the effective interaction $H_{\text{eff}}^{\text{I}}$ is due to the virtual transitions to the high energy states. Its matrix elements read

$$H_{\text{eff};ab}^{\text{I}} = \frac{1}{2} \sum_{\gamma \in \text{high}} \left(\frac{H_{a\gamma}^{\dagger} H'_{\gamma b}}{E_a - E_{\gamma}} + \frac{H_{a\gamma}^{\dagger} H'_{\gamma b}}{E_b - E_{\gamma}} \right). \quad (\text{B9})$$

In this case the Hamiltonian can be up to a constant term recast by using the spin operators to the form of the 2CK model

$$H_{\text{eff}}^{\text{I}} = H_{2\text{CK}} = J_e \mathbf{S} \cdot \mathbf{s}_e + J_o \mathbf{S} \cdot \mathbf{s}_o, \quad (\text{B10})$$

where the s_{α} for $\alpha = e, o$ denote the spin densities which read

$$\mathbf{S} = \frac{1}{2} \sum_{ss'} d_s^{\dagger} \boldsymbol{\sigma}_{ss'} d_{s'} \quad (\text{B11})$$

for d -orbital and likewise for orbitals α , where $\boldsymbol{\sigma}$ is the vector whose components σ^i are the Pauli matrices. The coupling constant to the even channel is

$$J_e = 2V^2 \left(\frac{1}{-\epsilon} + \frac{1}{\epsilon + U} \right). \quad (\text{B12})$$

For the odd channel we get

$$J_o = 2V^2 g^2 \left(\frac{1}{-\epsilon + \Omega} + \frac{1}{\epsilon + U + \Omega} \right), \quad (\text{B13})$$

where the Ω in the denominators occur since high-energy states involve one excited phonon.

For the exponential modulation the hybridization parts read

$$\begin{aligned} H'_e &= V \cosh(gx) v_e, \\ H'_o &= V \sinh(gx) v_o. \end{aligned} \quad (\text{B14})$$

The low-energy Hamiltonian is again that of the 2CK model and the coupling constants read

$$J_e = 2V_s^2 \sum_{m=0}^{\infty} \left(\frac{\delta_m^e}{-\epsilon + m\Omega} + \frac{\delta_m^e}{\epsilon + U + m\Omega} \right), \quad (\text{B15})$$

$$J_o = 2V_s^2 \sum_{m=0}^{\infty} \left(\frac{\delta_m^o}{-\epsilon + m\Omega} + \frac{\delta_m^o}{\epsilon + U + m\Omega} \right), \quad (\text{B16})$$

where $\delta_m^{e,o} = |\langle 0 | (e^{gx} \pm e^{-gx}) / 2 | m \rangle|^2 = \exp(g^2) g^{2m} / m!$ for m even (odd) and zero otherwise, respectively.

Appendix C: CONDUCTANCE

The linear response conductance for a general interacting system is given by the Kubo formula⁵⁰

$$G = \lim_{\omega \rightarrow 0} \frac{e^2}{\omega} \text{Im} C_{II}^R(\omega), \quad (\text{C1})$$

where

$$C_{II}^R(\omega) = -i \lim_{\eta \rightarrow 0} \int_0^{\infty} [I(t), I(0)] e^{i(\omega + i\eta)t} dt \quad (\text{C2})$$

is the retarded current-current correlation function and the current operators are defined by the time derivative of the electrons in the leads

$$I = \frac{\dot{N}_R - \dot{N}_L}{2}. \quad (\text{C3})$$

For Fermi liquid systems at $T = 0$ the current-current correlation function can be expressed in terms of the Green's function $G_{nn'}(\omega)$ involving sites n, n' in the leads. The conductance is then given by the Landauer formula (Fisher-Lee relation⁵¹)

$$G = G_0 |t(\omega)|^2, \quad (\text{C4})$$

where $G_0 = 2e^2/h$ is the quantum of conductance and the transmission amplitude $t(\omega)$ can be written as^{52,53}

$$t(\omega) = \frac{1}{-i\pi\rho(\omega)} e^{-ik(n-n')} G_{n'n}(\omega + i\eta). \quad (\text{C5})$$

Alternatively, the transmission amplitude can be expressed also in terms of the scattering matrix $S_{\alpha\alpha'}$ which relates the amplitudes of the outgoing wave in lead α to the amplitude of the incoming wave in the lead α'

$$S = \begin{pmatrix} r_L & t_R \\ t_L & r_R \end{pmatrix}, \quad (\text{C6})$$

where r_{α} (t_{α}) are the respective reflection and transmission coefficients. The scattering matrix can be rotated in the L-R space to the basis of channels (linear combinations of left and right states) where it is diagonal⁵⁴

$$USU^{-1} = \begin{pmatrix} e^{i2\delta_a} & 0 \\ 0 & e^{i2\delta_b} \end{pmatrix}, \quad (\text{C7})$$

where $U = \exp(i\theta\tau_y) \exp(i\alpha\tau_z)$ and τ_i are the Pauli matrices. According to the Landauer formula Eq. (C4) the zero-temperature conductance is determined by the transmission probability $t(0) = S_{RL} = t_L$, hence we obtain

$$G/G_0 = \sin^2(\delta_a - \delta_b) \sin^2(2\theta). \quad (\text{C8})$$

The angle θ determines the maximal value of conductance. In the inversion symmetric case $\theta = \pi/4$, the

phase-shifts δ_α which occur in the even and odd channels can then be extracted from the NRG finite-size spectra⁵⁵.

When the system is not inversion symmetric it is not possible to extract θ since the channel indices are not tracked. To evaluate the conductance in this case we resort to equation Eq. (C1). The current operator $I = (\dot{N}_L - \dot{N}_R)/2$ is obtained by commuting $N_\alpha = \sum_{k\sigma} n_{k\alpha\sigma}$ with the Hamiltonian for $\alpha = L, R$ and reads

$$\dot{N}_{L(R)} = -\frac{i}{\hbar}(1 \mp gx)V \sum_{\sigma} (c_{1L(R)\sigma}^\dagger d - h.c.), \quad (\text{C9})$$

where $c_{1L(R)\sigma}^\dagger$ creates an electron in the orbital next to impurity in the left(right) lead, respectively.

Alternatively, the conductance can be calculated also from the dependence of the ground state energy on auxiliary magnetic flux^{33,34,56,57} which is obtained by embed-

ding the interacting system into auxiliary noninteracting ring and threading the ring with magnetic flux Φ . Then the conductance can be expressed as^{33,34}

$$G/G_0 = \sin^2 \left[\frac{\pi}{2} \frac{E(\pi) - E(0)}{\Delta} \right], \quad (\text{C10})$$

where $E(\Phi)$ is the ground state energy of the auxiliary ring with embedded interacting system and $\Delta = 1/(\rho(\epsilon_F)N)$ the level spacing in the auxiliary ring with the density of states at the Fermi energy $\rho(\epsilon_F)$ which consists of N sites. This approach is useful especially in connection to variational approaches [such as SG, although in SG we can extract the conductance also from Eq. (C4) directly and obtain same results], where the ground state energy is the most reliable quantity.

-
- ¹ D. Goldhaber-Gordon, H. Shtrikman, D. Mahalu, D. Abusch-Magder, U. Meirav, and M. A. Kastner, **391**, 156 (1998).
- ² V. Madhavan, W. Chen, T. Jamneala, M. F. Crommie, and N. S. Wingreen, *Science* **280**, 567 (1998).
- ³ W. Liang, M. P. Shores, M. Bockrath, J. R. Long, and H. Park, *Nature* **417**, 725 (2002).
- ⁴ J. Park, A. N. Pasupathy, J. I. Goldsmith, C. Chang, Y. Yaish, J. R. Petta, M. Rinkoski, J. P. Sethna, H. D. Abrunas, P. L. McEuen, et al., *Nature* **417**, 722 (2002).
- ⁵ L. H. Yu and D. Natelson, *Nano Lett.* **4**, 79 (2005).
- ⁶ A. N. Pasupathy, J. Park, C. Chang, A. V. Soldatov, S. Lebedkin, R. C. Bialczak, J. E. Grose, L. A. K. Donev, J. P. Sethna, D. C. Ralph, et al., *Nano Lett.* **5**, 203 (2005).
- ⁷ A. Zhao, Q. Li, L. Chen, H. Xiang, W. Wang, S. Pan, B. Wang, X. Xiao, J. Yang, J. G. Hou, et al., *Science* **309**, 1542 (2005).
- ⁸ L. H. Yu, Z. K. Keane, J. W. Ciszek, L. Cheng, J. M. Tour, T. Baruah, M. R. Pederson, and D. Natelson, *Phys. Rev. Lett.* **95**, 256803 (2005).
- ⁹ C. A. Balseiro, P. S. Cornaglia, and D. R. Grempel, *Phys. Rev. B* **74**, 235409 (2006).
- ¹⁰ M. D. N. Regueiro, P. S. Cornaglia, G. Usaj, and C. A. Balseiro, *Phys. Rev. B* **76**, 075425 (2007).
- ¹¹ P. S. Cornaglia, G. Usaj, and C. A. Balseiro, *Phys. Rev. B* **76**, 241403 (2007).
- ¹² A. Nitzan and M. A. Ratner, *Science* **300**, 1384 (2003).
- ¹³ N. J. Tao, *Nature Nanotech.* **1**, 173 (2006).
- ¹⁴ M. Galperin, M. A. Ratner, and A. Nitzan, *J. Phys.: Condens. Matter.* **19**, 1 (2007).
- ¹⁵ N. Roch, S. Florens, V. Bouchiat, and W. W. F. BALESTRO, *Nature* **453**, 633 (2008).
- ¹⁶ S. Barišić, J. Labbé, and J. Friedel, *Phys. Rev. Lett.* **25**, 919 (1970), the idea of modulation of tunneling by displacement is neither new nor applies only to mesoscopic systems, see, *e.g.*,
- ¹⁷ P. Nozières and A. Blandin, *J. Phys. (France)* **41**, 193 (1980).
- ¹⁸ J. Mravlje, A. Ramšak, and R. Žitko, *Physica B* **403**, 1484 (2008).
- ¹⁹ A. C. Hewson and D. Meyer, *J. Phys: Condens. Matter* **14**, 427 (2002).
- ²⁰ J. Mravlje, A. Ramšak, and T. Rejec, *Phys. Rev. B* **72**, 121403(R) (2005).
- ²¹ J. Mravlje, A. Ramšak, and T. Rejec, *Phys. Rev. B* **74**, 205320 (2006).
- ²² T. Novotný, A. Donarini, C. Flindt, and A.-P. Jauho, *Phys. Rev. Lett.* **92**, 248302 (2004).
- ²³ H.-S. G. J. Twamley, D. W. Utami and G. Milburn, *New J. Phys.* **8**, 63 (2006).
- ²⁴ J. R. Johansson, L. G. Mourokh, A. Y. Smirnov, and F. Nori, *Phys. Rev. B* **77**, 035428 (2008).
- ²⁵ J. Koch, M. E. Raikh, and F. von Oppen, *Phys. Rev. Lett.* **96**, 056803 (2006).
- ²⁶ M.-J. Hwang, M.-S. Choi, and R. López, *Phys. Rev. B* **76**, 165312 (2007).
- ²⁷ M. N. Kiselev, K. Kikoin, R. I. Shekhter, and V. M. Vinokur, *Phys. Rev. B* **74**, 233403 (2006).
- ²⁸ K. G. Wilson, *Rev. Mod. Phys.* **47**, 773 (1975).
- ²⁹ R. Bulla, T. A. Costi, and T. Pruschke, *Rev. Mod. Phys.* **80**, 395 (2008).
- ³⁰ R. Žitko and J. Bonča, *Phys. Rev. B* **74**, 045312 (2006).
- ³¹ K. Schönhammer, *Phys. Rev. B* **13**, 4336 (1976).
- ³² O. Gunnarsson and K. Schönhammer, *Phys. Rev. B* **31**, 4815 (1985).
- ³³ T. Rejec and A. Ramšak, *Phys. Rev. B* **68**, 033306 (2003).
- ³⁴ T. Rejec and A. Ramšak, *Phys. Rev. B* **68**, 035342 (2003).
- ³⁵ M. Fabrizio, *Lectures on the physics of strongly correlated systems* (AIP, 2007), chap. I, p. 3.
- ³⁶ I. Affleck, A. W. W. Ludwig, H.-B. Pang, and D. L. Cox, *Phys. Rev. B* **45**, 7918 (1992).
- ³⁷ R. Bulla, T. A. Costi, and D. Vollhardt, *Phys. Rev. B* **64**, 045103 (2001).
- ³⁸ A. C. H. R Bulla and T. Pruschke, *J. Phys: Condens. Matter* **10**, 8365 (1998).
- ³⁹ G. S. Jeon, T.-H. Park, and H.-Y. Choi, *Phys. Rev. B* **68**, 045106 (2003).
- ⁴⁰ P. D. Sacramento and P. Schlottmann, *Phys. Rev. B* **40**, 431 (1989).
- ⁴¹ H.-U. Desgranges and K. D. Schotte, *Phys. Lett.* **91A**, 240

- (1982).
- ⁴² V. T. Rajan, J. H. Lowenstein, and N. Andrei, Phys. Rev. Lett. **49**, 497 (1982).
- ⁴³ A. Georges, G. Kotliar, W. Krauth, and M. J. Rozenberg, Rev. Mod. Phys. **68**, 13 (1996).
- ⁴⁴ L. Y. Gorelik, A. Isacsson, M. V. Voinova, B. Kasemo, R. I. Shekhter, and M. Jonson, Phys. Rev. Lett. **80**, 4526 (1998).
- ⁴⁵ H. G. Craighead, Science **290**, 1532 (2000).
- ⁴⁶ A. N. Cleland, J. S. Aldridge, D. C. Driscoll, and A. C. Gossard, Appl. Phys. Lett. **81**, 1699 (2002).
- ⁴⁷ N. E. Flowers-Jacobs, D. R. Schmidt, and K. W. Lehnert, Phys. Rev. Lett. **98**, 096804 (2007).
- ⁴⁸ C. B. Doiron, B. Trauzettel, and C. Bruder, Phys. Rev. Lett. **100**, 027202 (2008).
- ⁴⁹ P. Coleman, *Lectures on the physics of strongly correlated electron systems VI* (American Institute of Physics, 2002), vol. 629, chap. 2, pp. 79–160.
- ⁵⁰ W. Izumida, O. Sakai, and Y. Shimizu, J. Phys. Soc. Jpn. **66**, 717 (1997).
- ⁵¹ D. S. Fisher and P. A. Lee, Phys. Rev. B **23**, 6851 (1981).
- ⁵² A. Oguri, J. Phys. Soc. Jpn. **66**, 1427 (1997).
- ⁵³ A. Oguri, J. Phys. Soc. Jpn. **70**, 2666 (2001).
- ⁵⁴ M. Pustilnik and L. I. Glazman, Phys. Rev. Lett. **87**, 216601 (2001).
- ⁵⁵ L. N. Oliveira and J. W. Wilkins, Phys. Rev. B **24**, 4863 (1981).
- ⁵⁶ V. Meden and U. Schollwöck, Phys. Rev. B **67**, 035106 (2003).
- ⁵⁷ R. A. Molina, D. Weinmann, R. A. Jalabert, G.-L. Ingold, and J.-L. Pichard, Phys. Rev. B **67**, 235306 (2003).